Journal of Sol-Gel Science and Technology (2024) 111:966–978
https://doi.org/10.1007/s10971-024-06496-5

ORIGINAL PAPER

# First principles study to investigate structural, optical properties and bandgap engineering of $XSnI_3$(X=Rb, K, Tl, Cs) materials for solar cell applications

Muhammad Hasnain Jameel[1,2] · Alaa Nihad Tuama[3] · Aqeela Yasin[4] · Mohd Zul Hilmi Bin Mayzan[1,2] · Muhammad Sufi bin Roslan[2] · Laith H. Alzubaidi[5]

Accepted: 18 July 2024 / Published online: 31 July 2024


## Abstract

The PBE-GGA (Perdew Burke-Ernzerhof Generalized Gradient Approximation) for the exchange-correlation potentials, based on first-principles density functional theory (DFT) study is used to investigate the structural, optical, and electrical aspects of $XSnI_3$ (X = Rb, K, Tl, and Cs) materials. According to the DFT calculation, the energy band gaps ($E_g$) of $XSnI_3$ (X = Rb, K, Tl, and Cs) materials are 2.76, 2.01, 1.90, and 0.34 eV respectively. The direct energy bandgap ($E_g$) indicates that halide perovskite materials are appropriate semiconductors for solar cell application. A thorough analysis of optical conductivity indicates that, the optical conductance peaks of $XSnI_3$ (X = Rb, K, Tl, and Cs) halide perovskite materials reach maximum values of 2.3, 2.2, 4.5, and 5.2 eV, respectively, in the ultraviolet spectrum and shift slightly at higher energy bands. The maximal optical conductivity of $XSnI_3$ (X = Rb, K, Tl, and Cs) materials were $(1.6 \times 10^5\ \Omega^{-1}\ cm^{-1}, 1.8 \times 10^5\ \Omega^{-1})\ cm^{-1}$, $2.2 \times 10^5\ \Omega^{-1}\ cm^{-1}$ and $2.4 \times 10^5\ \Omega^{-1}\ cm^{-1}$ respectively. The $XSnI_3$ (X = Rb, K, Tl, and Cs) is a group of materials with enhanced surface area for light photon absorption and enhanced optical conductivity, energy absorption, and refractive index properties make them suitable for perovskite solar cell application.

## Graphical Abstract

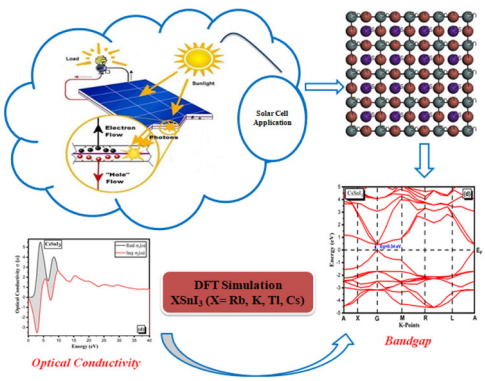


✉ Muhammad Hasnain Jameel
mhasnainjamil@gmail.com

✉ Mohd Zul Hilmi Bin Mayzan
zulhilmi@uthm.edu.my

[1] Ceramic and Amorphous Group (CerAm), Faculty of Applied Sciences and Technology, Pagoh Higher Education Hub, Universiti Tun Hussein Onn Malaysia, Panchor, Johor, Malaysia

[2] Department of Physics and Chemistry, Faculty of Applied Sciences and Technology (FAST), Universiti Tun Hussein Onn Malaysia, 84600 Pagoh, Johor, Malaysia

[3] Department of Physics, College of Education for Pure Sciences, University of Babylon, 5001 Hillah, Iraq

[4] School of Materials Science and Engineering, and Henan Key Laboratory of Advanced Magnesium Alloy and Key Laboratory of Materials Processing and Mold Technology (Ministry of Education), Zhengzhou University, Zhengzhou, China

[5] College of Technical Engineering, the Islamic University, Najaf, Iraq

**Keywords:** Halide perovskites · Bandgap engineering · Solar cell applications

**Highlights**

- The PBE-GGA (Perdew Burke-Ernzerhof Generalized Gradient Approximation) for the exchange-correlation potentials, based on first-principles density functional theory (DFT) study is used to investigate the structural, optical, and electrical aspects of $XSnI_3$ (X = Rb, K, Tl, and Cs) materials.
- According to the DFT calculation, the energy band gaps ($E_g$) of $XSnI_3$ (X = Rb, K, Tl, and Cs) materials are 2.76, 2.01, 1.90, and 0.34 eV respectively.
- The direct energy bandgap ($E_g$) indicates that halide perovskite materials are appropriate semiconductors for solar cell application. A thorough analysis of optical conductivity indicates that the optical conductance peaks of $XSnI_3$ (X = Rb, K, Tl, and Cs) halide perovskite materials reach maximum values of 2.3, 2.2, 4.5, and 5.2 eV, respectively, in the ultraviolet spectrum and shift slightly at higher energy bands.
- The $XSnI_3$ (X = Rb, K, Tl, and Cs) is a group of materials with enhanced surface area for light photon absorption and enhanced optical conductivity, energy absorption, and refractive index properties make them suitable for perovskite solar cell application.

## 1 Introduction

As living standards grow and the world's population increases, technological innovation will play a major role in the requirement of the world's energy demand in the twenty-first century [1, 2]. The most sustainable, renewable, and environmentally friendly method of energy generation for meeting energy demands the appropriate approach is solar energy harvesting [3, 4]. Due to their fascinating optoelectronic features and high power conversion efficiency (PCE), halide perovskite-based solar cells have attracted the attention of scientists during the past decade. The halide perovskite solar cell is a highly efficient solar cell type owing to its greater absorption coefficient, low excitation binding energy, high charge carrier mobility, and longer charge carrier diffusion length [5–7]. Hybrid halide perovskites typically have the crystal structure $ABX_3$, where A stands for an organic or inorganic cation, B for a metal cation, and X for an halogen family anion. Because these halide perovskites are naturally abundant and reasonably priced, they are widely used in a variety of industrial fields [8–11]. Numerous characteristics, including low exciton binding energy, low non-radiative recombination, long charge diffusion length, excellent optical absorption coefficient, and effective device functionality contribute to their efficiency [12–15].

There is evidence in the literature that the metal or cation choice in the metal halide influences the halide perovskites' electrical properties, durability, and absorption capacity [16, 17]. Nevertheless, due to the fact that the other perovskite materials are toxic and may pollute the environment or degrade the ecosystem, their use has raised concerns about the environment [18, 19]. Different components have been substituted in the development of higher-performing solar cells based on perovskite. Tin iodide (SnI), is one of the more notable replacements. Due to their improved electrical characteristics reduced toxicity, and good optoelectronic capabilities related to the active layer's tunable bandgap feature, SnI-based halide perovskites have emerged as the most promising substitute for solar cell applications [20–23]. The smallest bandgap of Sn-based halide PSCs is found to be between 1.31 and 1.60 eV, according to theoretical simulations. Improved optical and electrical characteristics are displayed by Sn-based PSCs, including greater charge mobility and a power conversion efficiency of almost 30% [23–27].

Using a quantum mechanical technique, Paschal and colleagues have investigated the electrical, thermodynamic, and structural properties of the guanidinium tin halide perovskite $SnX_3$ (where X = Cl, Br, and I) via DFT [28–32]. According to their findings, the band gaps of the materials were 2.47, 1.78, and 3.0 eV, respectively. The narrowest bandgap is found in $C(NH_2)_3SnI_3$ at 1.78 eV. The structural and electrical characteristics of a $CsXCl_3$ perovskite photovoltaic solar cell (where X = Sn, Pb, or Ge) were determined by Idrissi et al. [33–35] using Quantum Expresso software. The $CsSnCl_3$ material was determined to have the lowest bandgap among the three configurations after analysis, making it suitable for solar cell deployment [36, 37]. When compared to Cs-based perovskites, their investigation showed Thus, Sn-based PSCs had better optical conductivity, better light absorption, and more flexibility. Sn-based perovskite solar cells have the potential to be a workable replacement for lead-based perovskite, which is toxic, and other types of solar cells. It has been demonstrated that changing X to a different metal atom improves the physical and chemical characteristics of the perovskite structures, which may enable their use in a variety of solar systems. In this study, we examine how specific metals dopants affect the optoelectronic, optical, and structural characteristics of the perovskite structures $XSnI_3$

(X = Rb, K, Tl, and Cs). The primary objective of the current work is to investigate the structural, and optical properties of $XSnI_3$ materials using computational modeling with the CASTEP software. To the best of our knowledge, not much research has been published on the study of the $XSnI_3$ structure, where X is cesium, thallium, rubidium, and potassium (Cs, Tl, Rb, and K). It is envisaged that such studies will lead to future experimental studies to exploit the significant potential of such materials in Sn-based PSCs application.

## 2 Computational methodology

CASTEP simulation software is used for first-principles calculations [38]. The GGA (General Gradient Approximation) method was used to simulate the geometric structure and determine the electrical structure. The generalized gradient method of Perdew, Burke, and Ernzerhof (PBE) is frequently used to compute the exchange-correlation between energy and electrons. USP (ultra-soft pseudo-potential) was used to determine the electrostatic interactions between the valence electron and the ionic core [39]. An elongation of the wave function results from the accretion of plane waves with a cut-off energy of 365.5 eV. In structural analysis, the total energy convergence is less than $-1.01 \times 10^5$ eV/atom and the self-consistent convergence value is assumed to be $(4.67 \times 10^{-4})$ eV/atom. The electrical configurations of tin, rubidium, potassium, thallium, and cesium are $[Kr]4d^{10}5s^25p^2$, $[Xe]5s^1$, $[Ar]4s^1$, $[Xe]4f^{13}6S^2$ and $[Xe]6s^1$ respectively. It is determined that the maximum stress is less than $5.20 \times 10^{-2}$ and the maximum Hellmann-Feynman force is $0.0004eV/\dot{A}$. The highest atomic displacement that might occur is less than $1.22 \times 10^{-2}$Å. The Monkhorst Pack grid, which is composed of $16 \times 16 \times 4$ k-points, was sampled using First Brillouin for structural optimization and electronic property computations. In the non-periodic direction, we used a vacuum of 35 Å is along the lattice vector to prevent undesired interactions. Fig. 1a–d presents the 2D supercell $(8 \times 8 \times 2)$ of $XSnI_3$ (X = Rb, K, Tl, and Cs) halide perovskite materials.

## 3 Results and discussion

### 3.1 Structural study

This section presents an analysis and presentation of the structural characteristics of the hybrid halide perovskites $XSnI_3$ (where X = Rb, K, Tl, and Cs). The three crystal lattice parameters were initially used for the unit cell geometry optimization. The x-alkali dopants (X = Rb, k, Tl, and Cs) are uniformly distributed along the matrix of the $SnI_3$. In the PBE-GGA approach the $XSnI_3$ (where X = Rb, K, Tl, and Cs) is simulated using the CASTEP simulation software. The atomic positions and space groups are displayed in Table 1. In the hybrid halide perovskite, the dopants are positioned at various corners of the orthorhombic crystal structure as shown in Fig. 1a–d. Our observed structural properties showed that the lattice parameters have an impact on the atomic locations of atoms in $XSnI_3$.

### 3.2 Electronic properties

Figure 2a–d displays the band structures and corresponding density of states graphs for $XSnI_3$ (where X = Rb, K, Tl, and Cs). The primary electronic structural factors that are essential for deriving out the materials' orbital overlaps (or energy levels) and their relaxation influences on the different energy levels are the total density of states (TDOS) and partial density of states (PDOS). The energy range in which an electron can exist (conduction band, C.B.) and the locations where electron availability is zero are both depicted by the electronic band structure. The fermi level (Ef) is set to zero eV since all calculations were performed at 0 K without considering the effects of the finite temperature. The fermi level categorizes the conduction band and the valence band. The valance band (V.B.) is located below the energy Fermi level ($E_f$) and the C.B. is positioned above $E_f$. The bandgap can be found by comparing the valance band maxima (VBM) and conduction band minima CBM. Understanding material behavior and differentiating between conductors, insulators, and semiconductors will be made simpler by examining the presence or absence of a bandgap.

The material could have an indirect bandgap or a direct bandgap, based on the band structure. A direct Eg is observed when the VBM and CBM match. An indirect Eg is indicated when these two points are precisely off from one another. As illustrated in Fig. 2a–d, it has been found that the $E_g$ of the $XSnI_3$ (where X = Rb, K, Tl, and Cs) shows a decreasing trend with values as 2.76, 2.01, 1.90, and 0.34 eV obtained for $RbSnI_3$, $KSnI_3$, $TISnI_3$, and $CsSnI_3$ respectively. According to Fig. 2a–d, the VBM and CBM of the $XSnI_3$ materials under investigation are located at different symmetry locations, indicating both direct and indirect energy band gaps ($E_g$). In particular, VBM and CBM of $RbSnI_3$ and $KSnI_3$ halide perovskite material are situated at the same position M consistent with a direct Eg. However, the VBM and CBM in $TISnI_3$ are positioned at distinct places, indicating that $TISnI_3$ is an indirect semiconductor material. The VBM and CBM for $CsSnI_3$ are shown to be positioned at the same G point in Fig. 2d, indicating a direct semi-conducting material. The absorption of light increases from $1.7 \times 10^5\ cm^{-1}$ to $2.50 \times 10^5\ cm^{-1}$,

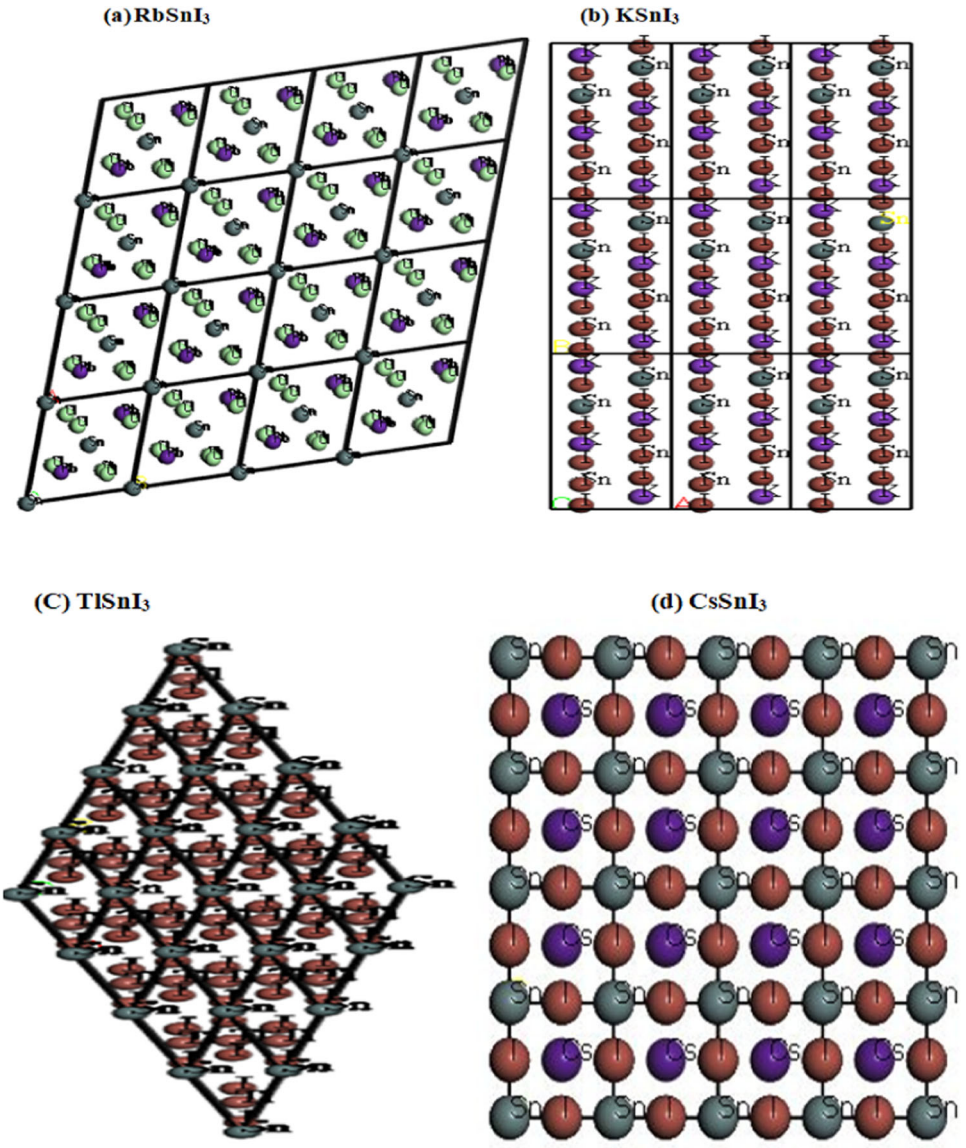


**Fig. 1** **a–d** Supercell of hybrid halide perovskite material XSnI3 (where X = Rb, K, Tl, and Cs)

**Table. 1** The XSnI3 supercell of structure materials' space groups, atomic locations, and lattice characteristics

| Materials | Lattice parameters (Å) | | | Atomic positions | | | | Space group | Structure |
|---|---|---|---|---|---|---|---|---|---|
| | | | | Atoms | a | b | c | | |
| $RbSnI_3$ | a = 4.791 | b = 10.573 | c = 17.636 | **Rb** | 0.25 | 0.0844 | 0.672 | Pnma | Orthorhombic |
| | | | | **Sn** | 0.25 | 0.8378 | 0.672 | | |
| | | | | **I** | 0.25 | 0.1997 | 0.288 | | |
| $KSnI_3$ | a = 3.691 | b = 3.691 | c = 3.691 | **K** | 0.25 | 0.4192 | 0.827 | Pnma | Orthorhombic |
| | | | | **Sn** | 0.25 | 0.6618 | 0.439 | | |
| | | | | **I** | 0.25 | 0.1588 | 0.946 | | |
| $TlSnI_3$ | a = 7.948 | b = 7.948 | c = 11.920 | **Tl** | 0.246 | 0.754 | 0.25 | Cmcm | Orthorhombic |
| | | | | **Sn** | 0 | 0 | 0 | | |
| | | | | **I** | 0.0789 | 0.9211 | 0.75 | | |
| $CsSnI_3$ | a = 8.773 | b = 8.872 | c = 12.663 | **Cs** | 0.0047 | 0.0233 | 0.25 | Pnma | Orthorhombic |
| | | | | **Sn** | 0 | 0.5 | 0.5 | | |
| | | | | **I** | 0.0026 | 0.52 | 0.75 | | |

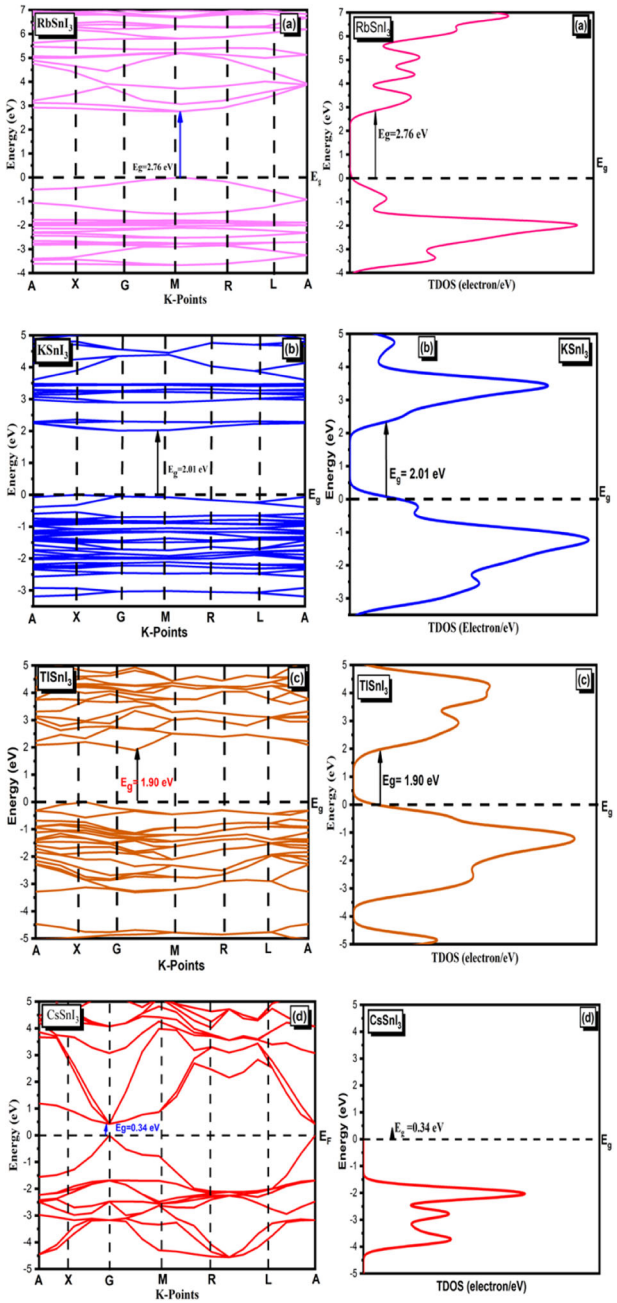


**Fig. 2** **a–d** Bandgap structures and TDOS of $XSnI_3$ (where X = Rb, K, Tl, and Cs)

and optical conductivity increases from 1.6 to 2.4 eV, as the bandgap decreases from 1.76 to 0.34 eV as shown in Table 2. The TDOS is used to measure the electronic bandgap represented per unit of energy regardless of how the partial density of states is used to analyze the contribution of ions to different band structures. With an Eg value of 0.34 eV, Fig. 4d demonstrates that the s state for the $CsSnI_3$ halide perovskite material contributes more to the conduction band than the p, d, and f states. This is explained by the higher sigma state contribution in the bandgap reduction. Because

**Table 2** The bandgap ($E_g$), absorption coefficient, and optical conductivity of halide perovskite materials

| Halide perovskite materials | | | | |
|---|---|---|---|---|
| Materials name | $RbSnI_3$ | $KSnI_3$ | $TlSnI_3$ | $CsSnI_3$ |
| Energy Bandgap ($E_g$) eV | 2.76 | 2.01 | 1.90 | 0.34 |
| Absorption Coefficient α(w) ($cm^{-1}$) | $1.7 \times 10^5$ | $1.9 \times 10^5$ | $2.1 \times 10^5$ | $2.50 \times 10^5$ |
| Optical Conductivity $\sigma_1 \times 10^3$ ($\Omega^{-1}\,cm^{-1}$) | $1.6 \times 10^3$ | 1.8 | 2.2 | 2.4 |

of its lower bandgap value, $CsSnI_3$ halide perovskite could be a desirable choice for solar cell applications.

The decrease in the bandgap is explained by the TDOS and PDOS. The dotted line represents the $E_f$ fermi level, which is located at the valence band's peak. These TDOS charts demonstrate that in $RbSnI_3$, $KSnI_3$, $TlSnI_3$, and $CsSnI_3$, recently produced extra gamma states are responsible for the bandgap decrement as shown in Fig. 3a–d. The C.B. shifted towards the $E_F$ along the G positioned as a result of newly produced gamma states of $XSnI_3$ materials is a significant factor in decreasing the $E_g$ of these materials. In semiconductors, these materials exhibit a direct-to-indirect bandgap structure, as demonstrated by the bandgap structures.

The data show that the "s" states highlighted in red contribute the most to C.B. for each material. However, in the s states, there are more gamma states. Consequently, s states contribute greater as compared to p and d states as shown in Fig. 4a–d. Figure 4a shows that the "s" state (in red color) is contributing more in the conduction band for the $RbSnI_3$ halide perovskite material with an $E_g$ value of 2.76 eV. Figure 4b shows that for the $KSnI_3$ halide perovskite material with an Eg value of 2.01 eV, the "s" and "p" states (shown in red and green respectively) contribute more than the "d" state (shown in blue) in the conduction band. Figure 4c illustrates how the "s" and "p" states contribute more to the conduction band than the d for the $TlSnI_3$ halide perovskite material, with an $E_g$ value of 1.90 eV. The energy bandgap for $TlSnI_3$ and $CsSnI_3$ decreases due to an increase in the hybridization of s, p, and d states. These findings indicate that halide perovskites are suitable for solar cell application.

## 3.3 Optical properties

Halide perovskite materials exhibit remarkable optical characteristics and can be employed in solar cells and photocatalysis. The complex ε (ω) dielectric parameters can explain the behavior of halide perovskite materials such as $RbSnI_3$, $KSnI_3$, $TlSnI_3$, and $CsSnI_3$ in an electric field. In particular ε(ω), is composed of two elements, the real dielectric function (RDF) and the imaginary dielectric

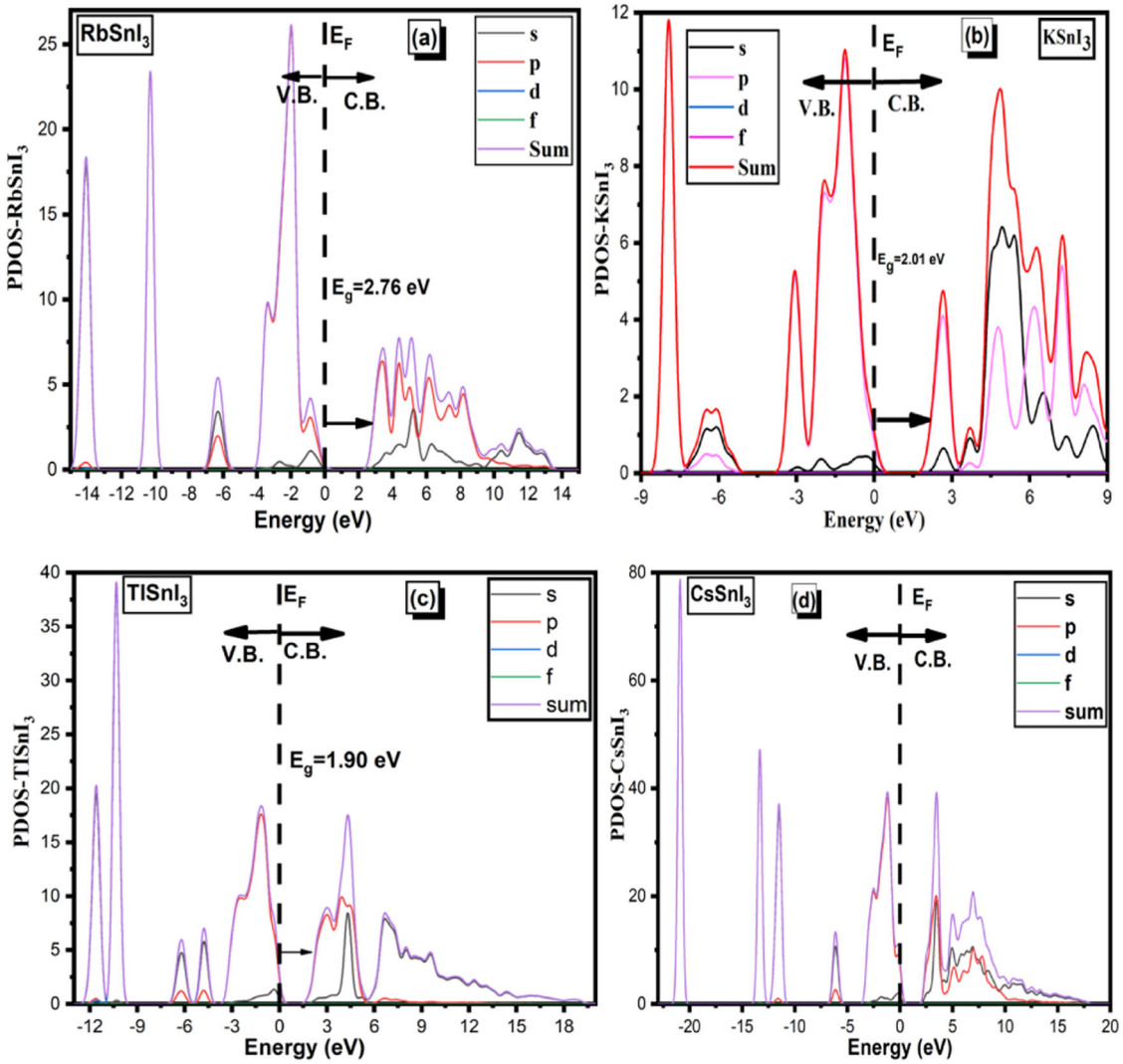


**Fig. 3** **a–d** Partial density of states XSnI3 (where X = Rb, K, Tl, and Cs)

function (IDF), and is based on a function of the optical band structure of the crystal. The electronic structure of halide perovskite materials such as $RbSnI_3$, $KSnI_3$, $TlSnI_3$, and $CsSnI_3$ can be used to define their optical properties, along with other features including the dielectric function, refractive index, coefficient of absorption, reflectivity, energy loss function, and optical conductivity. These characteristics are beneficial in indicating the materials' applicability and stability in solar cell applications.

The interaction between electromagnetic waves and valance electrons between the core electrons of $XSnI_3$ materials are responsible of all of the optical conductivity features. Since these characteristics are all related, the complex dielectric function can be expressed as follows [40–43].

$$\varepsilon(\omega) = \varepsilon_1(\omega) + i\varepsilon_2(\omega) \tag{1}$$

The optical response to the impact of $XSnI_3$ material hybridization on the dielectric function, which is quantifiable using the following formulas [44–48].

$$\varepsilon_2(\omega) = -\frac{Ve^2}{2\pi m^2\omega^2}\int d^3k \sum_{nn'} 1 < kn|P|k\tilde{n} > I^2 f(k) \times (1 - f(k\tilde{n})\delta(E_{kn} - E_{k\tilde{n}} - \omega) \tag{2}$$

The relative permittivity of $XSnI_3$ materials is given by the dielectric constants. The interpretation of the term "dielectric" explicitly, indicates the extent to which an electric field can pass through atoms of $XSnI_3$ materials. This primarily shows the maximum polarization that $XSnI_3$ material can withstand at different X atoms. Since there can never be a field inside the confines of an electrical conductor, the ideal conductor should have zero value. The terms are related to real part $[\varepsilon_1(\omega)]$, and the imaginary part $[\varepsilon_2(\omega)]$ within the $XSnI_3$ materials.

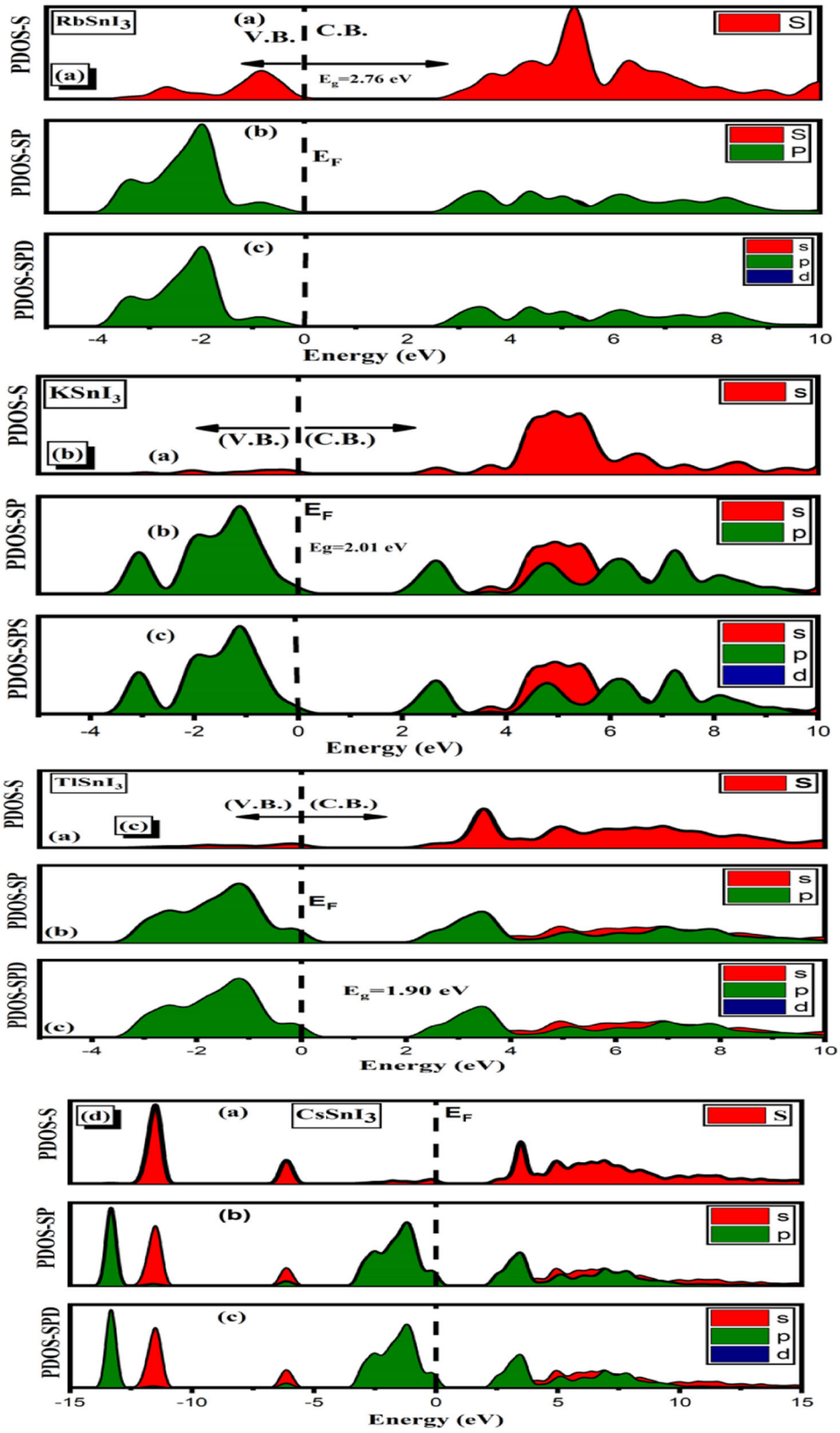


**Fig. 4 a–d** Partial density of states (PDOS) of RbSnI3, KSnI3, TISnI3, and CsSnI3 halide perovskite materials

As shown in Fig. 5a, the main peaks of $[\varepsilon_1(\omega)]$ have values of about 10, 4.3, and 2.4 respectively at 4 eV for $CsSnI_3$, $TISnI_3$, and $RbSnI_3$. In the case of $KsSnI_3$ the maximum value of >12 eV is observed at the 2 eV and then decreased to 2.3 near 4 eV. The peaks of the remaining halide perovskite materials started to drop after 5 eV as shown in Fig. 5b. With

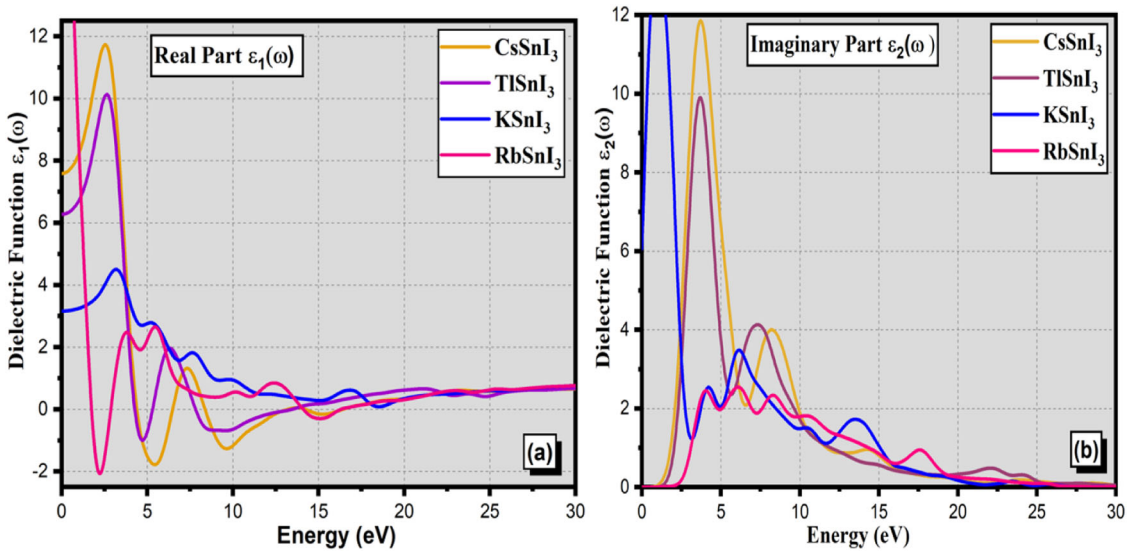


**Fig. 5** **a**, **b** The **a** real and **b** imaginary part of the dielectric functions of $RbSnI_3$, $KSnI_3$, $TlSnI_3$, and $CsSnI_3$halide perovskite materials Real (**a**) and imaginary (**b**) terms

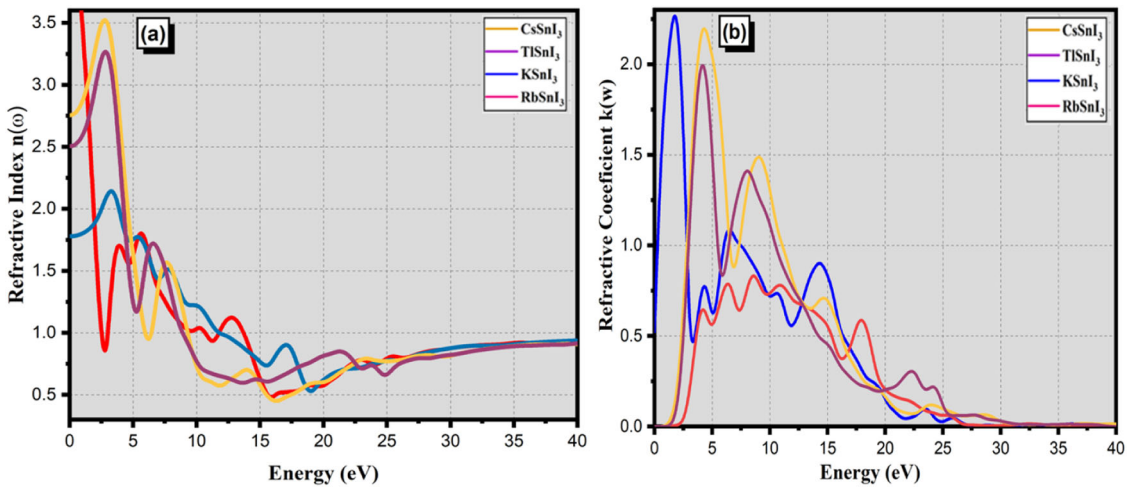


**Fig. 6** **a**, **b** Extinction coefficient and refractive index of $CsSnI_3$, $TlSnI_3$, $KSnI_3$, and $RbSnI_3$

Kramer's-Kronig mathematical formulation [49, 50], the RDF $[\varepsilon_1(\omega)]$ is formed by the IDF (imaginary dielectric function) $[\varepsilon_2(\omega)]$, as illustrated in Fig. 5b. For structures $CsSnI_3$, $TlSnI_3$, $KSnI_3$, and $RbSnI_3$, the maximum values of 11.8,10, 4.5, and 2.5 respectively are observed at 2.5–3 eV. Above 3 eV, the values of $\varepsilon_1(\omega)$ are shifted to lower values. These calculations suggest that these $XSnI_3$ halide perovskites are suitable for the solar cells industry.

### 3.3.1 Refractive index

Figure 6a, b displays the extinction coefficient (k(w)) and refractive index (n(w)) of the $XSnI_3$ halide perovskite material, which were carefully investigated. The results indicate optical transparency and capturing of electromagnetic (EM) wave radiations. The $\varepsilon_1(\omega)$ and $\varepsilon_2(\omega)$ dielectric functions dielectric vary with frequency in addition to providing a means of confirming the n(ω) complex refractive index provided by the following mathematical terms [51–54].

$$\tilde{n}(\omega) = n(\omega) + ik(\omega) = \epsilon^{1/2} = (\varepsilon_1 + i\varepsilon_2)^{1/2} \tag{3}$$

$$I(\omega) = \sqrt{2}\omega\left(\sqrt{\varepsilon_1(\omega)^2} + \sqrt{\varepsilon_2(\omega)^2} - \varepsilon_1(\omega)\right)^{1/2} \tag{4}$$

$$\sqrt{\varepsilon(\omega)} = n(\omega) + iK(\omega) = N(\omega) \tag{5}$$

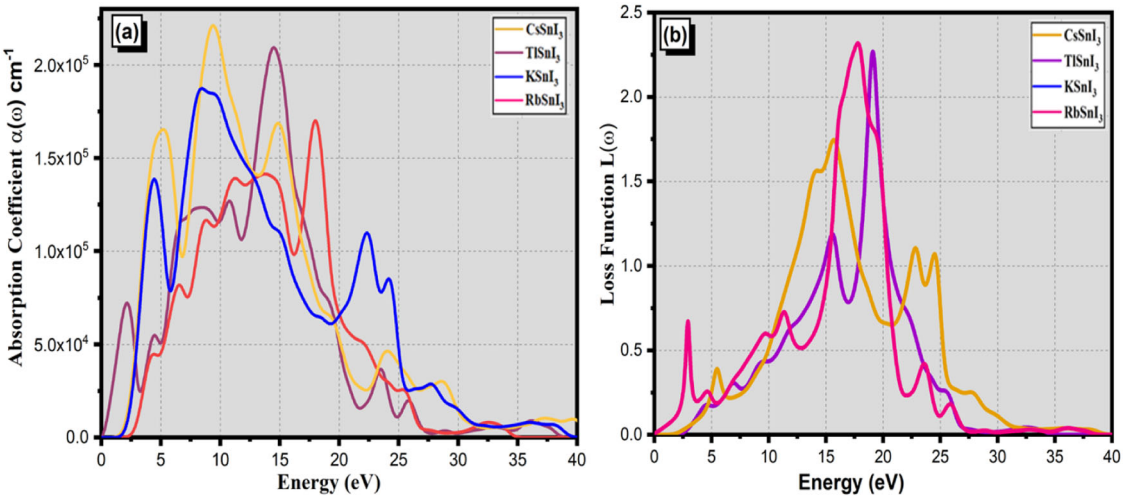


**Fig. 7** **a** Absorption coefficient **b** energy loss function for $CsSnI_3$, $TlSnI_3$, $KSnI_3$, and $RbSnI_3$

In this case, the imaginary extinction coefficient equation is presented by k(ω), whereas the real refractive index is commonly measured by n(ω) [5, 8, 55–57].

$$r(\omega) = \frac{n + iK - 1}{n + iK + 1} \tag{6}$$

$$K(\omega) = \frac{I(\omega)}{2\omega} \tag{7}$$

$$\varepsilon_2(\omega) = 2nK \tag{8}$$

$$\varepsilon_1(\omega) = n^2 - K^2 \tag{9}$$

The refractive index (n) at zero eV of the $XSnI_3$ samples is 1.7, 2.2, 3.4, and 3.5 for $RbSnI_3$, $KSnI_3$, $TlSnI_3$, and $CsSnI_3$ respectively. The refractive index peaks shifted toward a sharp decline with energy up to 5 eV. The refractive index (n) ranges from 0 to 5 in the energy range of 0–40 eV because of the different frequencies of the inner-transition band. In the prominent energy range, there is less polarization as indicated by the lower refractive index.

### 3.3.2 Absorbance and energy loss

The absorption quality of a material is directly related to its ability to absorb luminous electromagnetic radiation as opposed to photons with the appropriate energy, ($E = \hbar\omega$). Additionally, the energy loss function represented by $L(\omega)$ in Fig. 7b, describes the dissipation of incident photons energy in the materials. The following expression can be employed to address the absorption coefficient "$a(\omega)$" [58–61].

$$a(\omega) = 2\omega k(\omega) = \sqrt{2}[\{\varepsilon_1(\omega)^2 + \varepsilon_2(\omega)^2\}^{1/2} - \varepsilon_1(\omega)]^{1/2} \tag{9}$$

$$a(\omega) = \frac{4k\pi}{\lambda} = \frac{\omega}{nc}\varepsilon_2(\omega) \tag{10}$$

$$L(\omega) = \frac{\varepsilon_2}{\varepsilon_1(\omega)^2 + \varepsilon_2(\omega)^2} \tag{11}$$

The absorbance of $RbSnI_3$, $KSnI_3$, $TlSnI_3$, and $CsSnI_3$ is shown in Fig. 7a. Investigations have shown that light absorption is lowest in areas with roughly equal energy and maximum reflection. The capacity to absorb according to Fig. 7a, of halide perovskite materials containing $RbSnI_3$, $KSnI_3$, $TlSnI_3$, and $CsSnI_3$ is sharply rising. A slight shift toward higher energy values is observed in all of the absorption peaks. As illustrated in Fig. 7a, the absorption coefficient α(w) values are $2.4 \times 10^5\ cm^{-1}$, $2.2 \times 10^5\ cm^{-1}$, $1.9 \times 10^5\ cm^{-1}$, and $1.7 \times 10^5\ cm^{-1}$ for $CsSnI_3$, $TlSnI_3$, $KSnI_3$, and $RbSnI_3$ respectively. When compared to other materials $CsSnI_3$, and $TlSnI_3$, with absorption coefficients of $2.4 \times 10^5\ cm^{-1}$ and $2.2 \times 10^5\ cm^{-1}$, respectively, exhibit the maximum absorption. The absorption coefficient α(w) indicates a shift toward high absorbance in the range of 5 eV to 20 due to the notable decrease in energy bandgap. These absorption results indicate that the halide perovskite materials $CsSnI_3$, $TlSnI_3$, $KSnI_3$, and $RbSnI_3$ are suitable for solar cell applications.

### 3.3.3 Optical conductivity and reflectivity

The conductance of photo-generated electrons caused by the photoelectric process is characterized by optical

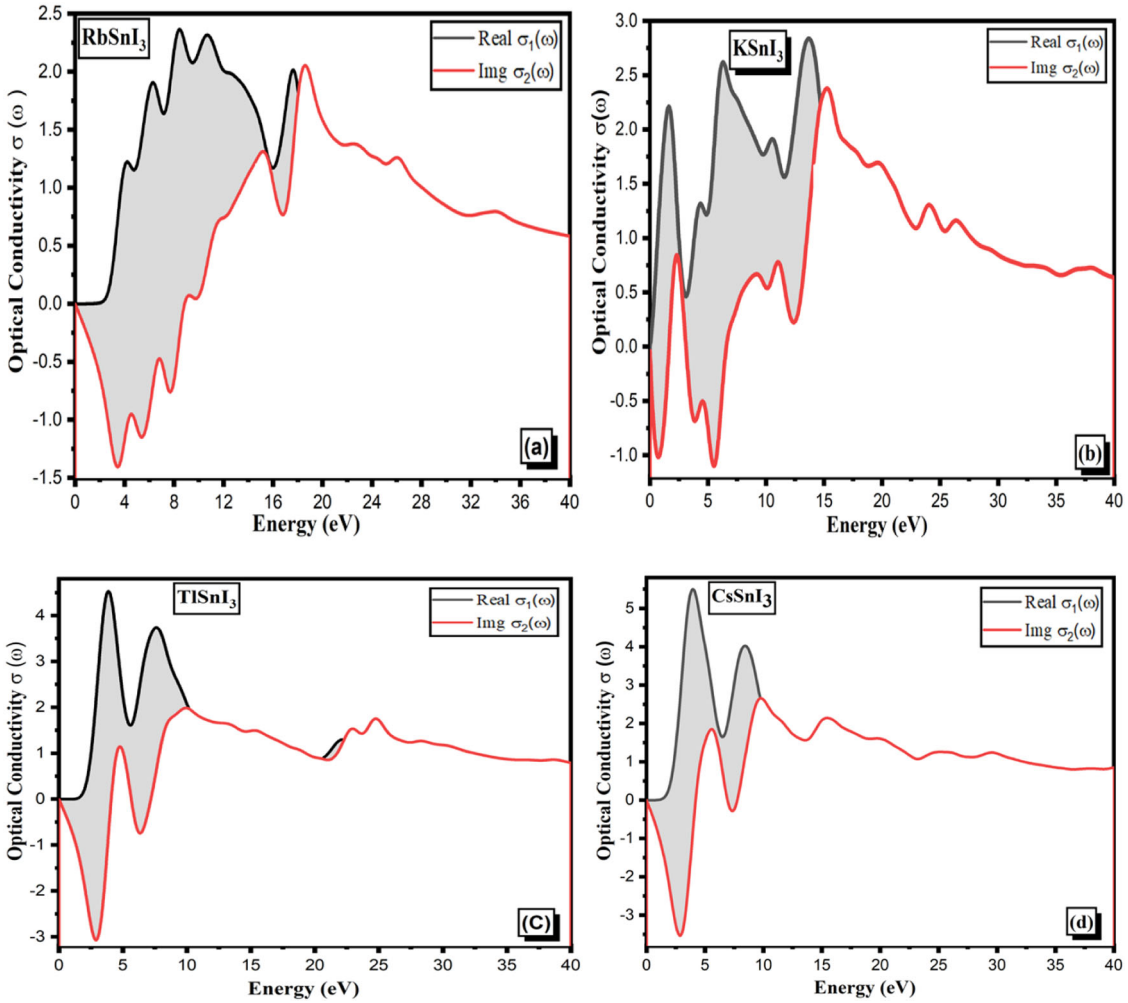


**Fig. 8** **a**, **d** Optical conductivity of **a** $RbSnI_3$ **b** $KSnI_3$ **c**$TlSnI_3$, and **d** $CsSnI_3$ halide perovskite materials

conductivity. Particle bonding is broken by electromagnetic radiation. The optical conductance of $CsSnI_3$, $TlSnI_3$, $KSnI_3$, and $RbSnI_3$ is displayed in Fig. 8a–d, covering the 0–40 eV range. The real peaks of optical conductance $\sigma_1(w)$ for $RbSnI_3$, $KSnI_3$, $TlSnI_3$, and $CsSnI_3$ are in the energy range of 0 to 20 eV and originate from the origin point and touch their maximum conductivity values of 2.3, 2.8, 4.5, and 5.2 eV respectively. The real component of their optical conductivities decreases steadily 40 eV reaching a maximum around at 5 eV. Conversely, the imaginary optical conductivity $\sigma_2(w)$ for the $RbSnI_3$, $KSnI_3$, $TlSnI_3$, and $CsSnI_3$ have maximum values at 5 eV of 2.1, 2.4, 2, and 2.6 $cm^{-1}$ respectively. The optical conductivity results suggest that $RbSnI_3$, $KSnI_3$, $TlSnI_3$, and $CsSnI_3$ are suitable materials for solar cell applications.

Any material's reflectivity can be utilized to analyze how its surface behaves. Figure 9 displays the surface reflectivity behavior of $TlSnI_3$, $CsSnI_3$, $KSnI_3$, and $RbSnI_3$. From 0 to 15 eV, the reflectivity peaks increased; however, they began to decrease at 16 eV as shown in Fig. 9. The reflectivity peaks of the $RbSnI_3$, $KSnI_3$, $TlSnI_3$, and $CsSnI_3$ halide perovskite materials are 0.15, 0.38, 0.42, and 0.62 respectively. The maximum reflectance peaks of 0.62 and 0.42 are observed in these two $CsSnI_3$ and $TlSnI_3$ materials when compared to other halide perovskite materials, $KSnI_3$ and $RbSnI_3$. $CsSnI_3$ and $TlSnI_3$ show improved absorption and optical conductivity compared to other materials. According to the results in Fig. 9, there is a slight shift in the reflectivity peaks toward higher energy levels.

## 4 Conclusion

Utilizing the Perdew Burke-Ernzerhof Generalized Gradient Approximation (PBE-GGA) for the exchange-correlation potentials, a density functional theory-based (DFT) study is used to investigate the structural, optical, and electrical aspects of $XSnI_3$ (X = Rb, K, Tl, and Cs) materials.

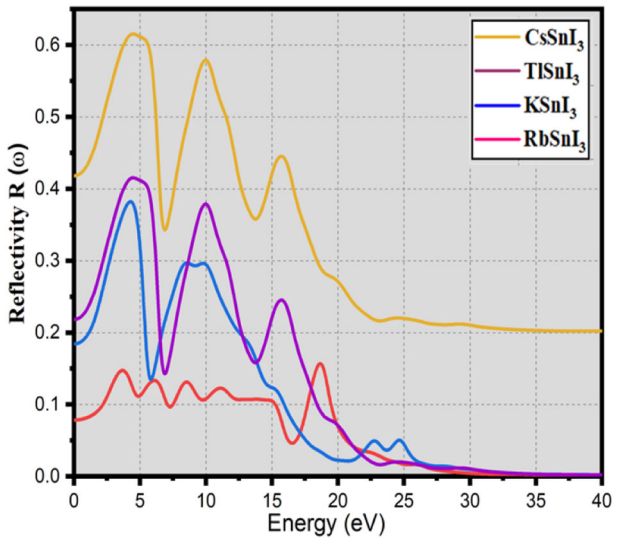


**Fig. 9** Optical reflectivity of $RbSnI_3$, $KSnI_3$, $TlSnI_3$, and $CsSnI_3$

According to the DFT calculation, the energy band gaps ($E_g$) of $XSnI_3$ (X = Rb, K, Tl, and Cs) materials are 2.76, 2.01, 1.90, and 0.34 eV respectively. The direct energy bandgap ($E_g$) indicates that these materials are appropriate semiconductors for solar cell application. A thorough analysis of optical conductivity indicates that the optical conductance peaks of $XSnI_3$ (X = Rb, K, Tl, and Cs) have maxima of 2.3, 2.8, 4.5, and 5.2 eV in the ultraviolet spectrum and shift slightly at higher energy bands. The maximal absorbance of $XSnI_3$ (X = Rb, K, Tl, and Cs) materials were $(1.4 \times 10^5\ \Omega^{-1}\ cm^{-1})$, $(1.8 \times 10^5\ \Omega^{-1}\ cm^{-1})$, $(2.2 \times 10^5\ \Omega^{-1}\ cm^{-1})$ and $(2.4 \times 10^5\ \Omega^{-1}\ cm^{-1})$ respectively. The $XSnI_3$ (X = Rb, K, Tl, and Cs) is a group of materials with enhanced surface area for light photon absorption. XSnI3 (X = Rb, K, Tl, and Cs) are suitable halide perovskites for solar cell applications due to their enhanced optical conductivity, energy absorption, and refractive index. The halide family has enormous promise for energy generation application. Additionally, current modeling studies are waiting experimental validation.

**Acknowledgements** This research is supported by Universiti Tun Hussein Onn Malaysia through grant Tier-1 (Q524).

**Author contributions** Muhammad Hasnain Jameel: Writing – original draft, Writing – review & editing, Data curation, Visualization, Investigation, Formal analysis, Methodology, Validation. Alaa Nihad Tuama: Writing – original draft, Writing – review & editing, Aqeela Yasin: Writing – review & editing, Mohd Zul Hilmi Bin Mayzan: Supervision, Review & editing. Muhammad Sufi bin Roslan: Writing – review & editing. Laith H. Alzubaidi: Review & editing.

## Compliance with ethical standards

**Conflict of interest** The authors declare no competing interests.

## References

1. Crabtree GW, Lewis NS (2007) Solar energy conversion. Phys Today 60(3):37–42
2. Fahrenbruch A, Bube R (2012) Fundamentals of solar cells: photovoltaic solar energy conversion. Elsevier.
3. Caid M, Rached D, Rached Y et al. (2024) Comprehensive exploration of halide double perovskites $Cs_2B'GeCl_6$ (B′: Zn, Cd) for affordable energy technologies: a high-throughput investigation. Opt Quant Electron 56:980. https://doi.org/10.1007/s11082-024-06721-z
4. Caid M, Rached D, Rached H et al. (2024) Structural, elastic, electronic, and optical properties of lead-free halide double perovskites $Cs_2B'B''Br_6$ (B'B": BeMg, CdBe, CdGe, GeMg, GeZn, MgZn): ab initio calculations. J Mol Model 30:59. https://doi.org/10.1007/s00894-024-05861-z
5. Tuama AN, Abass KH, Agam MAB (2021) Efficiency enhancement of nano structured Cu2O: Ag/laser etched silicon-thin films fabricated via vacuum thermal evaporation technique for solar cell application. Optik 247:167980
6. Abubakr M et al (2021) Study of structural, optoelectronic and magnetic properties of Half-Heusler compounds QEuPa (Q= Ba, be, Mg, Sr) using first-principles method J Solid State Chem 304:122612
7. Abbas Z et al. (2023) First-principles calculations to investigate electronic, optical, and thermoelectric properties of Na2GeX3 (X = S, Se, Te) for energy applications. Mater Sci Semicond Process 154(Nov):107206. https://doi.org/10.1016/j.mssp.2022.107206.
8. Tuama AN, Abassb KH, Agama MA (2020) Fabrication and Characterization of Cu2O:Ag/Si Solar Cell Via Thermal Evaporation Technique. Int J Nanoelectron Mater 13(3):601–614
9. Liu S, Guan Y, Sheng Y, Hu Y, Rong Y, Mei A, Han H (2020) A review on additives for halide perovskite solar cells. Adv Energy Mater 10(13):1902492
10. Xiao Z, Yan Y (2017) Progress in theoretical study of metal halide perovskite solar cell materials. Adv Energy Mater 7(22):1701136
11. Qiu L, Ono LK, Qi Y (2018) Advances and challenges to the commercialization of organic–inorganic halide perovskite solar cell technology. Mater Today Energy 7:169–189
12. Abbas Z et al. (2023) First-principles calculations to investigate structural, electronic, optical, elastic and thermodynamic properties of Yb3Q5 (Q=Ge, Si) for energy applications. Optik https://doi.org/10.1016/j.ijleo.2023.171493
13. Parveen A, Abbas Z, Hussain S, Shaikh SF, Aslam M, Jung J (2023) Theoretical justification of structural, magnetoelectronic and optical properties in QFeO3 (Q = Bi, P, Sb): a first-principles study. Micromachines https://doi.org/10.3390/mi14122251
14. Caid M, Rached D, Rached Y, Rached H (2024) "Exploring the versatile properties of Cs2B′GeF6 (B′: Sn, Pb) double perovskites: Insights into their mechanical stability, optoelectronic potential, and high thermoelectric performance." Phys B Condens Matter https://doi.org/10.1016/j.physb.2024.415742
15. Yin WJ, Yang JH, Kang J, Yan Y, Wei SH (2015) Halide perovskite materials for solar cells: a theoretical review. J Mater Chem A 3(17):8926–8942
16. Caid M, Djamel R, Habib R, and Youcef R (2024) A density functional theory exploration of Cs2B' B "I6 (B' B": BeCa, BeSr, GeCd, GeBe, GeMg) halide double perovskites for optimal solar cell and renewable energy applications. Phys Status Solidi (b) https://doi.org/10.1002/pssb.202300577
17. Zhao Z, Gu F, Rao H, Ye S, Liu Z, Bian Z, Huang C (2019) Metal halide perovskite materials for solar cells with long-term stability. Adv Energy Mater 9(3):1802671
18. Jaffery SHA et al. (2023) Strong interlayer transition in a staggered gap GeSe/MoTe2 heterojunction diode for highly efficient

visible and near-infrared photodetection and logic inverter. EcoMat 5(3):1–14. https://doi.org/10.1002/eom2.12307
19. Abubakr M et al. (2023) Systematic study on the optoelectronic and elastic properties of Cu-based ternary chalcogenides: using ab-initio approach. Mater Sci Semicond Process 162(Apr):107512. https://doi.org/10.1016/j.mssp.2023.107512
20. Ono LK, Juarez-Perez EJ, Qi Y (2017) Progress on perovskite materials and solar cells with mixed cations and halide anions. ACS Appl Mater Interfaces 9(36):30197–30246
21. Ono LK, Qi Y (2016) Surface and interface aspects of organo-metal halide perovskite materials and solar cells. J Phys Chem Lett 7(22):4764–4794
22. Caid M, Rached Y, Rached D, Rached H (2023) First principles study of the structural, elastic, magneto-electronic and thermo-electric properties of double perovskite Ba2ZrFeO6 in ferrimagnetic phase. Comput Condens Matter https://doi.org/10.1016/j.cocom.2023.e00847
23. Caid M, Rached D, Al-Qaisi S, Rached Y, Rached HJSSC (2023) DFT calculations on physical properties of the lead-free halide-based double perovskite compound Cs2CdZnCl6.". Solid State Commun 369:115216. https://doi.org/10.1016/j.ssc.2023.115216
24. Tombe S, Adam G, Heilbrunner H, Apaydin DH, Ulbricht C, Sariciftci NS, Scharber MC (2017) Optical and electronic properties of mixed halide (X= I, Cl, Br) methylammonium lead perovskite solar cells. J Mater Chem C 5(7):1714–1723
25. Shakil M, Akram A, Zeba I, Ahmad R, Gillani SSA, Gadhi MA (2020) Effect of mixed halide contents on structural, electronic, optical and elastic properties of CsSnI3− xBrx for solar cell applications: first-principles study. Mater Res Express 7(2):025513
26. Chakraborty K, Choudhury MG, Paul S (2021) Study of physical, optical, and electrical properties of cesium titanium (IV)-based single halide perovskite solar cell. IEEE J Photovolt 11(2):386–390
27. Caid M, Rached Y, Rached D et al. (2023) Theoretical insight of stabilities and optoelectronic properties of double perovskite $Cs_2CuIrF_6$: ab-initio calculations. J Mol Model 29:178. https://doi.org/10.1007/s00894-023-05588-3
28. Ogunwale GJ, Louis H, Amodu IO, Charlie DE, Ikot IJ, Olagoke PO, Adeyinka AS (2023) Modeling the structural, electronic, optoelectronic, thermodynamic, and core-level spectroscopy of X–SnO3 (X= Ag, Cs, Hf) perovskites. Comput Theor Chem 1220:114003
29. de Holanda MS, Moral RF, Marchezi PE, Marques FC, Nogueira AF (2021) Layered metal halide perovskite solar cells: a review from structure-properties perspective towards maximization of their performance and stability. EcoMat 3(4):e12124
30. Abate A, Saliba M, Hollman DJ, Stranks SD, Wojciechowski K, Avolio R, Snaith HJ (2014) Supramolecular halogen bond passivation of organic–inorganic halide perovskite solar cells. Nano Lett 14(6):3247–3254
31. Mirza SH, Azam S, Abbas Z et al. (2023) Enlightening the impact of TM doping on structural, electronic and magnetic properties of ceria for ReRAM applications: a GGA + U study. Chem Pap 77:5481–5494. https://doi.org/10.1007/s11696-023-02879-0
32. Jaffery SHA, Dastgeer G, Hussain M, Ali A, Hussain S, Ali M, Jung J (2022) Near-direct band alignment of MoTe2/ReSe2 type-II p-n heterojunction for efficient VNIR photodetection. Adv Mater Technol 7(10):2200026
33. Caid M, Habib R, Bentouaf A, Djamel R, Youcef R (2021) High-throughput study of the structural, electronic, and optical properties of short-period (BeSe) m/(ZnSe) n superlattices based on DFT calculations.". Comput Condens Matter 29:e00598. https://doi.org/10.1016/j.cocom.2021.e00598
34. Caid M, Rached D, Cheref O, Righi H, Rached H, Benalia S, Merabet M, Djoudi L (2019) "Full potential study of the structural, electronic and optical properties of (InAs) m/(GaSb) n superlattices." Comput Condens Matter 21:e00394. https://doi.org/10.1016/j.cocom.2019.e00394
35. Kawano Y, Chantana J, Nishimura T, Minemoto T (2020) Influence of halogen content in mixed halide perovskite solar cells on cell performances through device simulation. Sol Energy Mater Sol Cells 205:110252
36. Jiang X, Li H, Zhou Q, Wei Q, Wei M, Jiang L, Ning Z (2021) One-step synthesis of SnI2·(DMSO) x adducts for high-performance tin perovskite solar cells. J Am Chem Soc 143(29):10970–10976
37. Caid M, Rached D (2020) "First-principles calculations to investigate structural, electronic and optical properties of (AlSb) m/(GaSb) n superlattices." Mater Sci-Pol 38 no. 2:320–327. https://doi.org/10.2478/msp-2020-0027
38. Heo JH, Kim J, Kim H, Moon SH, Im SH, Hong KH (2018) Roles of SnX2 (X= F, Cl, Br) additives in tin-based halide perovskites toward highly efficient and stable lead-free perovskite solar cells. J Phys Chem Lett 9(20):6024–6031
39. Lim EL, Hagfeldt A, Bi D (2021) Toward highly efficient and stable Sn 2+ and mixed Pb 2+/Sn 2+ based halide perovskite solar cells through device engineering. Energy Environ Sci 14(6):3256–3300
40. Nishimura K, Kamarudin MA, Hirotani D, Hamada K, Shen Q, Iikubo S, Hayase S (2020) Lead-free tin-halide perovskite solar cells with 13% efficiency. Nano Energy 74:104858
41. Abdel-Shakour M, Chowdhury TH, Matsuishi K, Bedja I, Moritomo Y, Islam A (2021) High-efficiency tin halide perovskite solar cells: the chemistry of tin (II) compounds and their interaction with Lewis base additives during perovskite film formation. Sol RRL 5(1):2000606
42. Shahzad M, Naeem H, Yasin MW, Usman Z, Ali SS, Rizwan M (2024) "Developing the insight for systematic exploration of hydrogen storage in RbMgF3." Int J Hydrog Energy 64:148–157. https://doi.org/10.1016/j.ijhydene.2024.03.272
43. Rizwan M, Naeem H, Naeem Ullah HM et al. (2024) Fine band gap tuning via Sr incorporated $PbTiO_3$ for optoelectronic application: a DFT study. Opt Quant Electron 56:122. https://doi.org/10.1007/s11082-023-05775-9
44. Paschal C (2021). Tin halide perovskites: computational modeling of structural, electronic and thermodynamic properties towards solar cell applications, Doctoral dissertation. NM-AIST
45. Ayub A, Ullah HMN, Rizwan M, Zafar AA, Usman Z, Hira U (2024) Impact of Zn alloying on structural, mechanical anisotropy, acoustic speeds, electronic, optical, and photocatalytic response of KMgF3 perovskite material Mater Sci Semicond Process 173:108049
46. Idrissi S, Ziti S, Labrim H, Bahmad L (2021) Band gaps of the solar perovskites photovoltaic CsXCl3 (X= Sn, Pb or Ge). Mater Sci Semicond Process 122:105484
47. Pingak RK, Harbi A, Moutaabbid M, Johannes AZ, Hauwali NUJ, Bukit M, Ndii MZ (2023) Lead-free perovskites InSnX3 (X= Cl, Br, I) for solar cell applications: a DFT study on the mechanical, optoelectronic, and thermoelectric properties. Mater Res Express 10(9):095507
48. Lanzetta L, Webb T, Zibouche N, Liang X, Ding D, Min G, Haque SA (2021) Degradation mechanism of hybrid tin-based perovskite solar cells and the critical role of tin (IV) iodide. Nat Commun 12(1):2853
49. Zhao Z, Gu F, Li Y, Sun W, Ye S, Rao H, Huang C (2017) Mixed-organic-cation tin iodide for lead-free perovskite solar cells with an efficiency of 8.12%. Adv Sci 4(11):1700204
50. Nguyen BP, Jung HR, Ryu KY, Kim K, Jo W (2019) Effects of organic cations on carrier transport at the interface between perovskites and electron transport layers in (FA, MA) SnI3 solar cells. J Phys Chem C 123(51):30833–30841

51. Jameel MH et al. (2024) Bandgap Engineering and Tuning of Electronic and Optical Properties of Hetero-atomsdoped-Graphene Composites by Density Functional Quantum Computing for Photocatalytic Applications. Catal Letters https://doi.org/10.1007/s10562-023-04541-6
52. Hassanien AS, Sharma I (2019) Band-gap engineering, conduction and valence band positions of thermally evaporated amorphous Ge15-x Sbx Se50 Te35 thin films: Influences of Sb upon some optical characterizations and physical parameters. J Alloy Compd 798:750–763
53. Tuama AN, Al-Bermany E, Alnayli RS, Abass KH, Abdali K, Jameel MH (2024) A critical review of the evaluation of Sio2-incorporated Tio2 nanocomposite for photocatalytic activity. Silicon 16(6):2323–2340. https://doi.org/10.1007/s12633-024-02870-8
54. Teyssedre G, Laurent C (2005) Charge transport modeling in insulating polymers: from molecular to macroscopic scale. IEEE Trans Dielectr Electr Insul 12(5):857–875
55. Bouhmaidi S, Marjaoui A, Talbi A, Zanouni M, Nouneh K, Setti L (2022) A DFT study of electronic, optical and thermoelectric properties of Ge-halide perovskites CsGeX3 (X= F, Cl and Br). Comput Condens Matter 31:e00663
56. Giorgi G, Fujisawa JI, Segawa H, Yamashita K (2014) Cation role in structural and electronic properties of 3D organic–inorganic halide perovskites: a DFT analysis. J Phys Chem C 118(23):12176–12183
57. Mezan SO, Jabbar AH, Hamzah MQ, Tuama AN, Hasan NN, Roslan MS, Agam MA (2019) Synthesis, characterization, and properties of polystyrene/SiO2 nanocomposite via sol-gel process. In: AIP conference proceedings, vol 2151, no1. AIP Publishing
58. Jabbar AH, Mezan SO, Tuama AN, Hamzah MQ, Ameruddin ASB, Agam MA (2019) Enhanced bioactivity of polystyrene-silver nanocomposite (PS/Ag NCs)-an antimicrobial study. In: AIP Conference Proceedings, vol 2151, no 1. AIP Publishing
59. Hamzah MQ, Jabbar AH, Mezan SO, Tuama AN, Agam MA (2019) Fabrications of PS/TiO2 nanocomposite for solar cells applications. In: AIP Conference Proceedings, vol 2151, no 1. AIP Publishing
60. Abbas Z, Zafar Z, Raza HH, Parveen A, Shaikh SF (2024) Density-functional quantum analysis of optoelectronic, elastic, thermodynamic and hydrogen storage properties of AMgH3 (A= be, ca) perovskite-type hydrides: prospects for clean energy hydrogen-storage fuel and optoelectronic applications. Int J Hydrog Energy 60(Feb):212–228. https://doi.org/10.1016/j.ijhydene.2024.02.081
61. Fatima K, Abbas Z, Butt F, Butt K, Hussain S, Ali A, Al-Sehemi AG (2023) First-principles quantum analysis of promising double perovskites Z2SiF6 (Z = K, Li, na, rb) as prospective light harvesting materials: optoelectronic, structural and thermodynamic properties. Int J Quantum Chem 123(18):e27179